Graphical Abstract

Eliminating Bias in Pedestrian Density Estimation: A Voronoi Cell

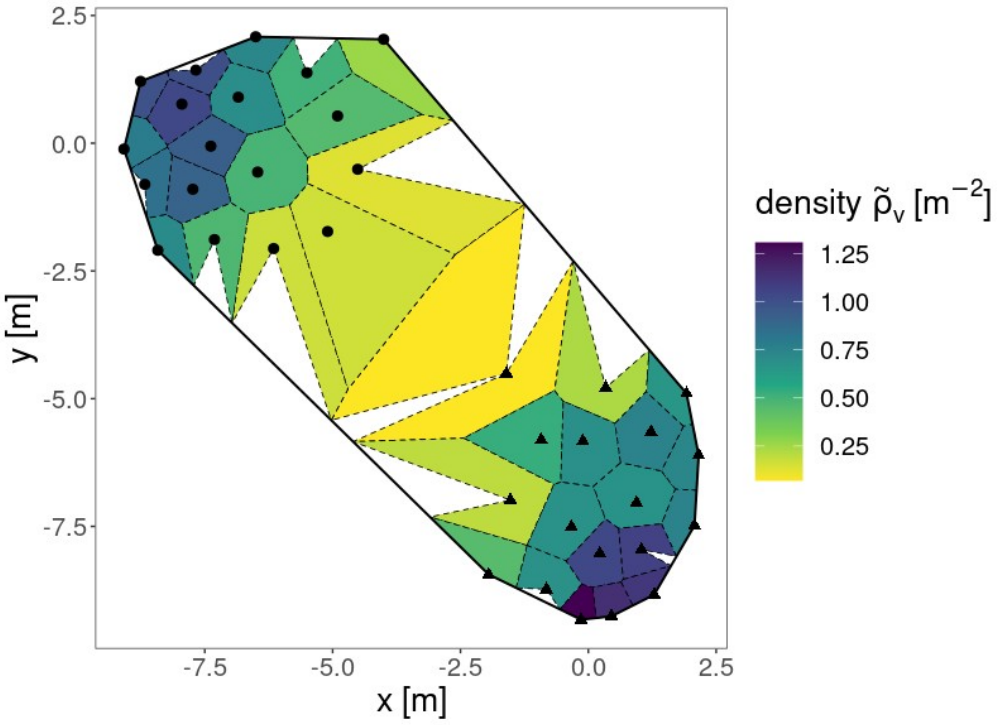

Density estimation for two groups (black circles and triangles) of pedestrians using modified voronoi cells (dashed lines) clipped by the convex hull (solid line).

Highlights

Eliminating Bias in Pedestrian Density Estimation: A Voronoi Cell Perspective

Pratik Mullick, Cécile Appert-Rolland, William H. Warren, Julien Pettré

- A Voronoi cell-based method for accurate density estimation in unbounded human groups.
- The method is applicable to pedestrian groups irrespective of their size.
- Precise individual-level density measurements, useful for effective crowd management.
- Provides a stable, parameter-independent, bias-free density estimation.

Eliminating Bias in Pedestrian Density Estimation: A Voronoi Cell Perspective

Pratik Mullick[a,b], Cécile Appert-Rolland[c], William H. Warren[d], Julien Pettré[b]

[a] *Department of Operations Research and Business Intelligence, Wrocław University of Science and Technology, Wyb. Wyspiańskiego 27, Wrocław, 50370, Lower Silesia, Poland*
[b] *Univ Rennes, INRIA, CNRS, IRISA, 263 Av. Général Leclerc, Rennes, 35042, Bretagne, France*
[c] *Université Paris-Saclay, CNRS/IN2P3, IJCLab, 15 Rue Georges Clemenceau, Orsay, 91400, Île-de-France, France*
[d] *Department of Cognitive, Linguistic and Psychological Sciences, Brown University, 190 Thayer Street, Providence, 02912, Rhode Island, USA*

Abstract

For pedestrians moving without spatial constraints, extensive research has been devoted to develop methods of density estimation. In this paper we present a new approach based on Voronoi cells, offering a means to estimate density for individuals in small, unbounded pedestrian groups. A thorough evaluation of existing methods, encompassing both Lagrangian and Eulerian approaches employed in similar contexts, reveals notable limitations. Specifically, these methods turn out to be ill-defined for realistic density estimation along a pedestrian's trajectory, exhibiting systematic biases and fluctuations that depend on the choice of parameters. There is thus a need for a parameter-independent method to eliminate this bias. We propose a modification of the widely used Voronoi-cell based density estimate to accommodate pedestrian groups, irrespective of their size. The advantages of this modified Voronoi method are that it is an instantaneous method that requires only knowledge of the pedestrians' positions at a give time, does not depend on the choice of parameter values, gives us a realistic estimate of density in an individual's neighborhood, and has appropriate physical meaning for both small and large human crowds in a wide variety of situations. We conclude with general remarks about the meaning of density measurements for small groups of pedestrians.

Keywords: pedestrian dynamics, crowd management, density estimation,

1. Introduction

Human crowd motion studies [1, 2, 3, 4, 5, 6, 7, 8] focus on understanding and modeling [9, 10] the behavior of individuals within large groups as they move through and interact with their environment. These studies are crucial for designing safer public spaces, optimizing evacuation procedures, and improving crowd management during events [11, 12, 13, 14, 15]. Human crowd motion is an example of a complex system because it involves numerous interacting agents (people) whose collective behavior cannot be easily predicted from the actions of individuals alone. Factors such as collective decision-making [16, 17, 18], social influences [19, 20, 21, 22], spatial constraints [23, 24], and environmental conditions [2, 25] lead to emergent phenomena, such as congestion [26, 27, 28, 29, 30, 31, 32], lane formation [33, 34, 35, 36, 37], and phase transitions between different flow states [38, 39, 40, 41, 42]. This complexity arises from the nonlinear interactions and adaptive behaviors exhibited by individuals, making crowd motion a rich field for exploring the principles of complex systems.

For efficient crowd management, a crucial aspect is the construction of a fundamental diagram (FD) [43, 44, 45, 46, 47, 48]. In the context of traffic flow, an FD basically depicts the relationship between traffic velocity and traffic density. This relationship could help to study the capacity of a space where the traffic moves, e.g., a road for vehicles, sidewalks for pedestrians. An FD could serve as a basic element of comprehensive models that describe the traffic operation on a network, thereby finding significant applications in the context of human traffic management and crowd safety [49, 50]. The FD could also be used as a valuable tool for assessing the capacity of pedestrian flow simulations to accurately predict real-world scenarios.

In this paper we will focus on the construction of an effective method for density estimation, based on the fact that density is most widely used in FDs.

Indeed, in the context of self-organizing behaviour of human crowd motion, methods of density estimation are an important topic of research [51, 52, 53, 54, 55, 56, 57, 58, 59, 60]. The existing literature consists of a number of methods, although the 'best'

method is unresolved and may depend on the crowd situation. Most of the research has focused on situations in which the moving crowd is constrained within a physical boundary, such as a corridor or sidewalk [61, 62]. For such cases, density estimation using a Voronoi tesselation [53, 63, 55, 34, 64] and a grid-based measure called the XT method [65, 66, 67] have been reported to work well. However, there is no well defined method of density estimation for groups in an unbounded space.

A further difficulty arises when the fundamental diagram, rather than being plotted at a global or meso scale [51], is related to individual quantities [68]. In one dimension, a proxy for density can be the inverse of the spatial headway with the predecessor. However, in two dimensions, finding a robust estimate of the density along the trajectory of a pedestrian is significantly more complex. Estimating local density in two-dimensional spaces requires capturing the spatial interactions among pedestrians accurately. The existing methods of density estimation often fall short in scenarios where pedestrian groups move in unbounded spaces or when the group size is relatively small. Our research introduces a density estimation method tailored to these specific conditions.

In [64] the authors developed a Voronoi cell based density estimation method for unbounded pedestrian groups in which the Voronoi cells are restricted to the angular sectors on the convex hull of the whole set of pedestrians. However, that method was demonstrated only for pedestrian groups larger than ~ 40 individuals. In our current paper we point out some typical cases that could arise when the pedestrian group is much smaller (~ 5). Our main contribution is a technique by which we can modify the Voronoi method to adjust the angular corrections for such small groups, and obtain a realistic estimate of the density field inside the group.With our added modification, the computational algorithm becomes more general and applicable to pedestrian groups of any size, even when the number of pedestrians is as small as 5.

In practical terms, this means that our method can dynamically adapt to the spatial distribution and movement patterns of pedestrians, offering a more realistic and bias-free estimate of local density. This is particularly important in unbounded environments, where traditional methods may struggle to account for the lack of spatial constraints. Our approach ensures that the density felt by an individual pedestrian is accurately captured, providing useful insights into crowd dynamics and interactions at a microscopic scale.

Furthermore, our method has the potential to enhance the construction of fundamental diagrams by providing precise density measurements at the individual level. This allows for a more detailed analysis of pedestrian behavior and flow characteristics, facilitating the development of more effective crowd management strategies and safety measures. By addressing the limitations of existing density estimation techniques, our proposed method represents a significant advancement in the study of human crowd motion and contributes to a deeper understanding of the complexities inherent in pedestrian dynamics.

The rest of the paper is organized as follows: in the next section we briefly describe the data set that has been used in this research to demonstrate our proposed computational algorithm. Then we briefly describe the existing methods of density estimation in the literature, and our proposal for adapting the Voronoi method for small groups without spatial boundaries. In the Results and Discussion section, we present an extensive evaluation of the earlier methods, which highlights their limitations and drawbacks. Then we show how our proposed method outperforms the previous methods in providing a bias-free realistic estimate of density in the neighborhood of an individual in small groups. We conclude with a general discussion on the meaning of defining a density at such small scales.

2. Materials and Methods

2.1. Experimental details

For this research, we consider the typical situation of crossing flows of pedestrians without any spatial constraints, where two groups of people walk across an open area from predefined initial positions such that their paths cross each other at specified values of the crossing angle. The data were obtained by experiments [69, 70] using live participants on the campus of University of Rennes, France. This data is available in a public repository `https://doi.org/10.5281/zenodo.5718430`. Two different sets of volunteered participants (36 on Day 1, 38 on Day 2) were roughly divided into two groups (18 or 19 per group) and were instructed to reach the other side of a sport hall. Initial positions were prescribed so that the groups had to cross each other with seven different crossing angles (0° to 180°, at 30° intervals). During each trial we recorded the head trajectory of each pedestrian as a time series at a frequency of 120 Hz using a motion capture system based on infrared cameras (VICON). The data obtained were then low-pass filtered

to decrease the oscillations due to the gait movement of the walking pedestrians. Precisely, we used a forward-backward 4th-order butterworth filter to these unwanted oscillations with a cut-off frequency of 0.5 Hz. In Figure 1 we show the traces of all the pedestrians for a typical trial using filtered trajectories.

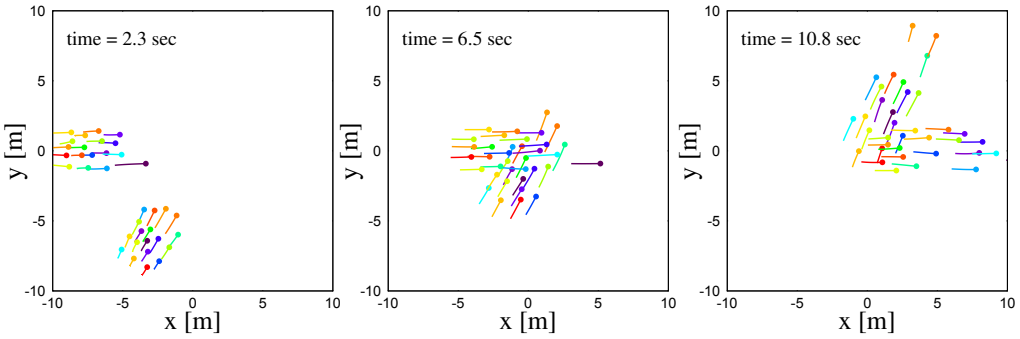

Figure 1: Displacements (1.25 sec) of all pedestrians in a typical trial with an expected crossing angle of 60°. The displacements are shown at three different time points, viz. 2.3 sec, 6.5 sec and 10.8 sec, from the beginning of the trial. The dots represent the pedestrians and the tails behind each dot are the distances travelled by the pedestrian in previous 1.25 sec.

2.2. Methods of density estimation

A large number of methods have been developed to measure the density field of pedestrian flows [53, 55]. In order to determine the fundamental diagram at an individual scale, one has to associate a density with a specific pedestrian location. In this subsection we briefly present three such methods which already exist in the literature in the context of pedestrian flows, followed by the Voronoi method [64] that we have modified to be applicable for pedestrian groups irrespective of their size. In the next section we shall evaluate the effectiveness of these methods.

2.2.1. Grid-based Classical Method

The classical method to estimate the density of pedestrians follows an Eulerian approach. In this method we divide the entire tracking region into a grid of square cells. If d_g is the length of one side of a square cell, the classical density ρ_g is given by

$$\rho_g = \frac{n}{d_g^2} \tag{1}$$

where n is the number of pedestrians that are located inside the square cell. The density estimated for each of the square regions is associated with all the pedestrians that are within the square. Note that sometimes, a single cell is used to measure density in a region of interest, such as in the crossing area of crossing flows [71, 72, 73].

In Figure 2 the density ρ_g fields of the pedestrians for a typical case in our data set has been shown for two typical values of d_g. Clearly the density

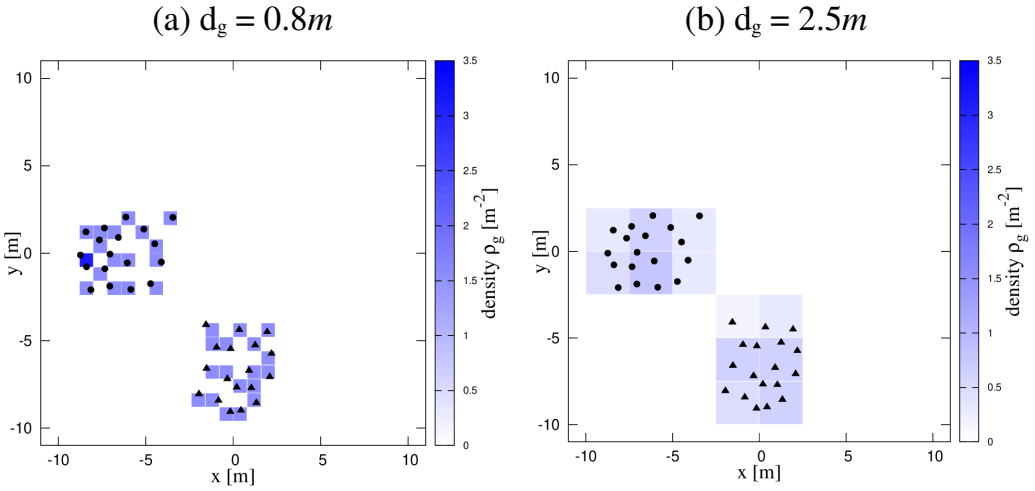

Figure 2: Density ρ_g fields as estimated using the grid-based classical method for two typical values of d_g , viz. (a) $d_g = 0.8$m and (b) $d_g = 2.5$s. Density values decrease with the increase in d_g . For this demonstration we use a typical data from our crossing flows data set. The two groups of people, denoted by black circles and triangles, attempt to cross each other at 90°. The group denoted by circles move along the x-axis from negative to the positive direction, whereas the group denoted by triangles move along the y-axis from negative to positive direction.

fields show variation with variation in d_g. Precisely, as d_g increases, density ρ_g values decreases **for a fixed number n of pedestrians, as could be seen from** Equation (1). In **Figure 8(a)** we show the time-sequence of classical density ρ_g for a typical pedestrian for several values of the cell size. For smaller cell sizes, the density values keep switching between only a few levels - which signifies the discrete nature of ρ_g.

2.2.2. XT Method

The XT method was originally proposed by Edie [65] in the context of traffic stream measurements, where the total distance travelled and the total

time spent by the pedestrian in a space-time region is taken into account. Edie's definition was extended [67] to be applicable to a three-dimensional space for multi-directional pedestrian motion. Later, this method was further modified [55], which we have used in this paper to compute the pedestrian density.

A square-shaped cell c of length d_x is considered at whose center a pedestrian p is located at time t, as shown in Figure 3. With the progression of

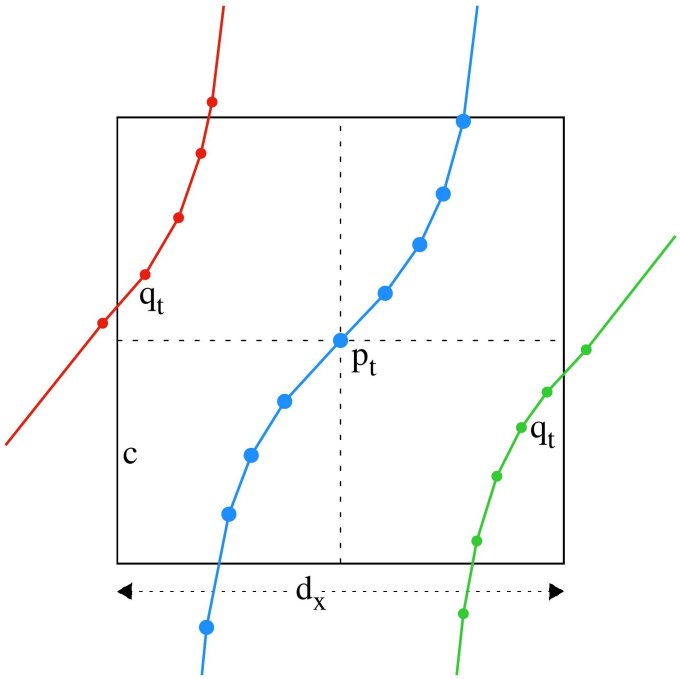

Figure 3: Schematic diagram showing the XT method to calculate the pedestrian density ρ_{xt}. The density calculated is associated to the pedestrian p_t , whose trajectory is shown in blue. At time t this pedestrian is located at the centre of the square shaped cell c of length d_x. Other pedestrians q_t, whose trajectories are shown in red and green also reside within this cell at time t and therefore are considered for density evaluations.

time, this cell travels with p, yielding the local density along the trajectory of p. This pedestrian-centered frame of reference contrasts with the classical method described previously, which has a space-centered frame of reference. There could be other pedestrians as well within this cell at time t. The density $\rho_{\mathrm{xt}}(c,t)$ estimated for this cell at time t is associated with the pedestrian

p and is given by

$$\rho_{\mathrm{xt}}(c,t) = \frac{\sum_q (T^q_{\mathrm{end}} - T^q_{\mathrm{begin}})}{{d_x}^2 \times T} \tag{2}$$

where the summation is performed over all the pedestrians q placed inside the cell c at time t. T^q_{begin} denotes either the time when the pedestrian q enters the cell c or the lower time boundary $t - 0.5T$, whichever is minimum

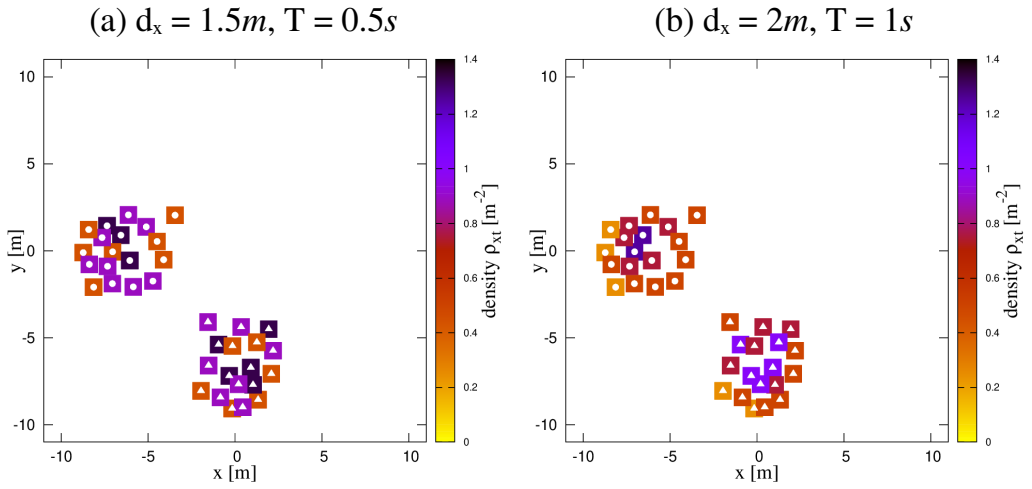

Figure 4: Density ρ_{xt} fields as estimated using the XT method for two sets of typical values of d_x and T , viz. (a) d_x = 1.5m, T = 0.5s and (b) d_x = 2m, T = 1s. Density values decrease with the increase in d_x and T. The data used here is the same one that has been used in Figure 2.

As mentioned earlier, the square shaped cell at time t (say) is fixed with a pedestrian p located at its center. Other pedestrians (denoted by q), throughout their trajectories could enter and exit this cell. Ideally it is possible that the same pedestrian enters and exits this cell multiple times, but it is highly unlikely for our case where there are not many sudden changes in trajectories in the crossing zone, or no direction reversals of pedestrian motions. In

the unlikely event that this is true, XT method considers the time spent within this cell for each time q enters and exits. For example, if a pedestrian q enters the cell at time T_1, exits at T_2, again enters at T_3 and exits at T_4, and enters for the last instance at time T_5 and finally exits at time T_6, then the numerator of Eq. (2) would be a sum of total time spent by this pedestrian into this cell, i.e., $(T_2 - T_1) + (T_4 - T_3) + (T_6 - T_5)$.

2.2.3. Kernel Method

To estimate the density of pedestrians in a two-dimensional unbounded space we also use a non-parametric method based on the kernel density estimator. **The term 'non-parametric' refers to the fact that the method does not make any statistical assumptions about the distribution of underlying data, for example, a normal distribution or any other particular shape of distribution.** This method basically evaluates the probability density function of the pedestrian positions, from which we calculate the density of pedestrians. Following a Lagrangian approach, this method gives an estimate of density even at the spatial positions where there are no data points.

For $\mathbf{X}_1, \mathbf{X}_2, \mathbf{X}_3, \ldots, \mathbf{X}_N$ to be the collection of two-dimensional coordinates for N pedestrians, the density function ρ_k estimated by the kernel density method at the spatial position $\mathbf{X}$ is given by

$$\rho_{\mathrm{k}}^{\mathbf{h}}(\mathbf{X}) = \sum_{i=1}^{N} K_{\mathbf{h}}(\mathbf{X} - \mathbf{X}_i), \tag{3}$$

where $\mathbf{h}$ is the bandwidth which dictates the smoothness of the density measurement. Among the several choices of the kernel function K, we use the bi-variate Gaussian distribution function given by,

$$K_{\mathbf{h}}(\mathbf{X}) = \frac{1}{2\pi}|\mathbf{h}|^{-\frac{1}{2}} e^{-\frac{1}{2}\mathbf{X}^T\mathbf{h}^{-1}\mathbf{X}} \tag{4}$$

In two dimensions $\mathbf{h}$ is supposed to be a 2×2 matrix that would contain a vector of bandwidths for the two dimensions to control the amount and orientation of smoothness. However, following the R adaptation of two dimensional kernel density estimator we use a scalar value as the bandwidth h that was taken to apply to both directions. From the estimated function $\rho_k(\mathbf{X})$, we finally estimate the density at each of the pedestrian positions and

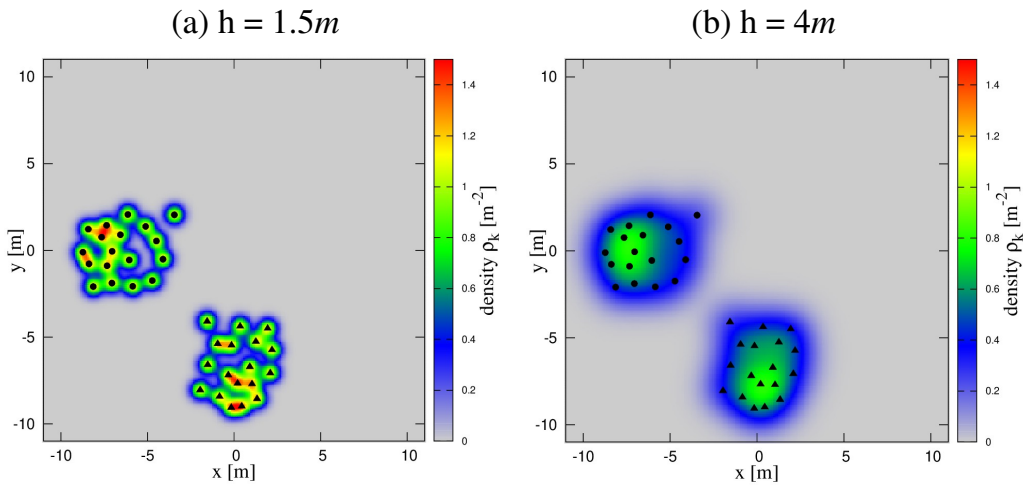

Figure 5: Density ρ_k fields as estimated using the kernel method for two typical values of the bandwidth, viz. (a) $h = 1.5$m and (b) $h = 4$m. Density values decrease with the increase in h. The data used here is the same one that has been used in Figures 2 and 4.

2.2.4. Voronoi Method

The Voronoi cell of a pedestrian P is the area A of the surface within which all the points are closer to P than to any other pedestrian P'. The density estimate of a pedestrian is then

$$\rho_v = \frac{1}{A}. \tag{5}$$

If we directly use this definition to construct the Voronoi diagram of the pedestrians at every instant of the trial, we notice that pedestrians on the edge of the groups may have a large and possibly infinite Voronoi cell leading to a density near zero. While this indicates that these pedestrians are not constrained by neighbors at least on one side, it may be more appropriate to associate with them the density on the group side.

If the group was confined in a space limited by physical boundaries, the latter could be used to bound the Voronoi cells. In the absence of such boundaries, a possibility is to bound Voronoi cells with an arbitrary limit.

For example a restriction to 2m^2 was used in [53], but for a wide variety of real-life situations there is no justified unique choice of this restriction. Here we prefer a method that depends on the density on the group side.

To do this, a first correction proposed in [64] is to restrict the Voronoi cells to the angular sectors in which the Voronoi cell lies inside the convex hull encompassing the whole set of pedestrians. In Figure 6(a) we have demonstrated a typical case for a randomly generated pedestrian group where the angular sectors, denoted by α, for each Voronoi-cell are shown. A correction in the density accounting for the suppressed angular sectors $2\pi - \alpha$ must be performed as

$$\tilde{\rho}_v = \frac{\alpha}{2\pi}\frac{1}{A} \tag{6}$$

where α is the angular sector on which the Voronoi cell is defined. This takes care of the angular adjustments for the agents located 'on' the convex hull and the agents whose Voronoi cell extend beyond the convex hull. The density values shown in Figure 6(a) are estimated by using Eq. (6).

However, for very small samples as the ones in our data set, there are some specific cases that have to be taken into account. For example, a Voronoi cell can extend on multiple sides of the group, requiring to suppress multiple sectors. One such example for a typical data set from our experiments is illustrated in Figure . The Voronoi cell corresponding to one of the pedestrians (P_2 at 0.8 sec) subtends 2 angular sectors with the convex hull. For such cases, Equation (6) can not be applied to find the density.

For even smaller group of pedestrians, the number of such multiple sectors could increase. In Figure 6(b) we show a randomly generated pedestrian group of 5 where the Voronoi cell of a pedestrian clipped by the convex hull extends along 3 directions. Another typical case for smaller pedestrian groups could be a pedestrian lying on the convex hull itself, but its Voronoi cell extends beyond the convex hull in the other direction, as shown in Figure 6(c). For both the cases shown in Figures 6(b) and 6(c), Eq. (6) becomes invalid for density estimation.

For these cases in which multiple angular sectors must be suppressed, we propose the following modification of Equation (6): as

$$\tilde{\rho}_v = \frac{\sum_i \alpha_i}{2\pi}\frac{1}{A} \tag{7}$$

where $i(> 1)$ is the number of problematic angular sectors that are clipped, as described above. The density values shown in Figures. 6(b) and 6(c)

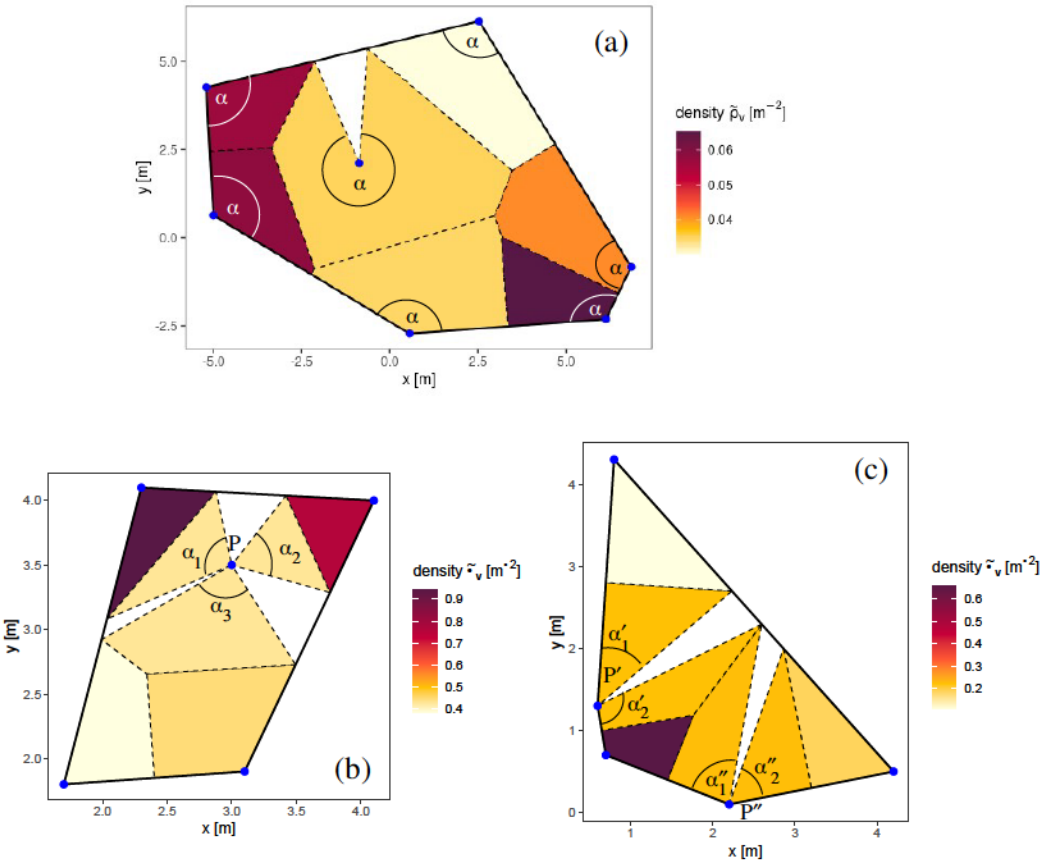

Figure 6: Examples of angular modifications in pedestrian groups. In each of the above panels the data correspond to randomly generated pedestrian positions, denoted by blue dots. The solid line in black denotes the convex hull for the group of pedestrians, and the dashed black lines indicate the Voronoi-cell boundaries. (a) A typical case with 7 pedestrians, where the angular sectors denoted by α are shown for each Voronoi-cell. (b) A typical case with 5 pedestrians, where pedestrian P's Voronoi cell is clipped by the convex hull in 3 directions, leading to multiple angular sectors, where $\alpha = \alpha_1 + \alpha_2 + \alpha_3$. (c) A typical case with 5 pedestrians, where pedestrians P' and P'' lie on the convex hull, and their Voronoi-cells are clipped by the convex hull in the opposite direction. This results in two angular sectors for each case, with $\alpha = \alpha'_1 + \alpha'_2$ and $\alpha = \alpha''_1 + \alpha''_2$.

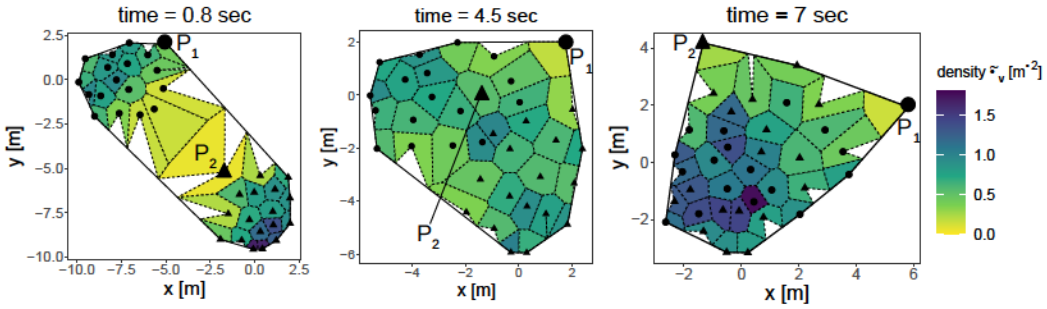

Figure 7: Modified Voronoi cells for a trial with a 90° crossing angle at three different instances. The black line represents the current convex hull. Dots and triangles in black indicate pedestrians from two groups, moving along the x-axis and y-axis respectively. Dotted lines mark the Voronoi cell boundaries. The entire video of this experimental trial with modified Voronoi cells is available as a supplementary material (S1 Video). The time-sequence of density estimations for pedestrians denoted by P_1 (bigger black dot) and P_2 (bigger black triangle) are shown in Figure 10. Pedestrian P_2 at time 0.8 sec is an example whose Voronoi cell extends in 2 directions to the convex hull, requiring suppression of two angular sectors. The entire video of this trial along with the modified Voronoi cells is provided as a supplemental online material (S1 Video).

were estimated by applying Equation (7). Notably, when there are multiple angular sectors to consider, application of Equation (6) would not be possible at all to estimate density, and Equation (7) has to be included in the computational algorithm.

Although the data set that we are primarily working with has $36 - 38$ pedestrians, during the time evolution of the two groups crossing each other, or in any other pedestrian situation in general, such peculiar cases occur and our computational strategy pertains to them. The code used for the Voronoi method with angular modifications is also available in the public repository `https://doi.org/10.5281/zenodo.8138327`, along with the crossing flows data set `https://doi.org/10.5281/zenodo.5718430`.

3. Results and Discussion

In the first three methods described in the previous section, the parameters d_g, d_x, or h determine the typical spatial length on which the presence of a pedestrian has an effect on the density when measuring the density field. It also determines the density value at the pedestrian location when density is measured along a trajectory. In Figure 8 we show how the density along the trajectory of a given pedestrian measured by the 3 aforementioned methods

varies as the spatial parameters d_g, d_x, or h decrease. We shall see in this

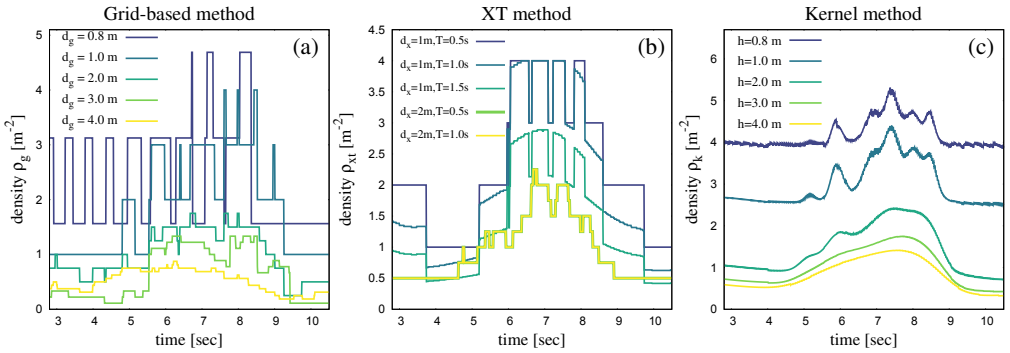

Figure 8: Temporal variations of density as a function of time, along the trajectory **pedestrian P_1 in Figure 7**. Density is determined by (a) the classical grid-based method, (b) the XT-method, (c) the Gaussian kernel method. Time sequences are shown for several values of the spatial scale d_g, d_x, or h and in (b), of the time window T.

section that, while some methods estimate the pedestrian density without any difficulty, others completely fail once they are used to determine density along a trajectory.

We first illustrate how this failure occurs using a classical grid-based method. As we are interested in situations with small number of pedestrians, d_g must be small enough to capture the immediate vicinity of a given pedestrian. In the limit of small cells, at most one pedestrian can be contained in the cell. The corresponding density is $\rho_{\max} \equiv 1/d_g^2$. If we plot the whole density field, we get typically a figure as in Figure 9(a) with some empty cells and some cells with density $\rho_{\max}$. The density field is not smooth, but using a spatial average, we get a reasonable density estimate - provided the area on which we average is homogeneous. For stationary flows, it is also possible to average in time even for a rather small measurement area [63] and to get average density values with rather low fluctuations.

Now instead, if we decide to measure the density along the trajectory of a given pedestrian, the density in the cell where this pedestrian is located will always be $\rho_{\max}$ - a value which can be arbitrarily high. Any kind of averaging will always give $\rho_{\max}$ (red line in Figure 9(b)), which is very far from the real average density value found previously (green line in Figure 9(b)). Actually density values are completely biased by the fact that we have selected cells conditionally, along the pedestrian trajectory.

Another variant could be to measure the density along the trajectory

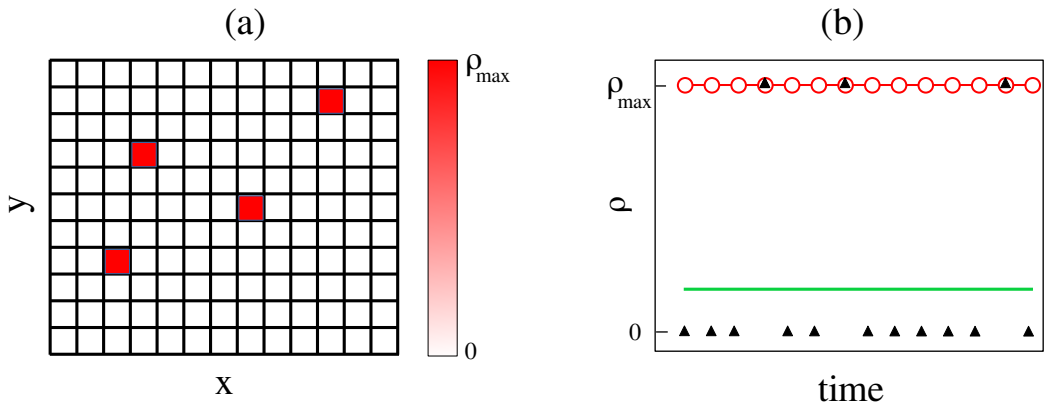

Figure 9: Sketch representing the variation in density estimated by the grid-based classical method (a) when the whole density field is plotted, (b) for a time evolution in a fixed cell (black triangles) or along a pedestrian trajectory (red circles). Solid line in red and green indicate the average values.

of a pedestrian without counting the pedestrian himself. But then again we encounter a bias: for small cells, the density along the trajectory would always be zero, far from the real density value. This grid-based method could be used to estimate the local density around the pedestrian trajectory only if the cell size could be chosen large compared to the inter-pedestrian distance, but small compared to density gradients. This is obviously not possible for the small pedestrian groups, similar to the ones involved in our experiment.

A similar failure for density measurements along trajectories can be observed for the next two methods as well, viz. XT method and Kernel method. The systematic bias and the fluctuations around this biased value have been studied in detail for one-dimensional systems in [58].

So to summarise for the first three methods, the effect of decreasing the spatial parameters d_g, d_x, or h is two-fold: fluctuations increase, and the average value increases towards arbitrarily high values. While the increase of fluctuations could possibly be reduced by more averaging, the bias introduced in the average value cannot be avoided and makes these methods ill-defined for a measurement along a pedestrian trajectory.

On the other hand, there are some methods that do not have the problem of bias along pedestrian trajectories as we discussed so far. These are the methods which, by definition, scan the surroundings of a pedestrian on a scale such that the nearest neighbors' positions can be taken into account. Among the various methods having this property, we here focus on Voronoi

method - a method which is very popular due precisely to its good behavior in a large range of situations [53, 63, 55, 34, 64], in spite of the fact that some fluctuations are introduced by the piece-wise constant nature of the density field. In the previous section we have described how this method can be adapted to account for small system sizes. In Figure 10 the variations of ρ_v (density obtained by original Voronoi method, Equation (5)) and $\tilde{\rho}_v$ (considering modified Voronoi cells clipped within the convex hull with sector suppression, Equation (7)) as a function of time have been plotted for 2 typical pedestrians.

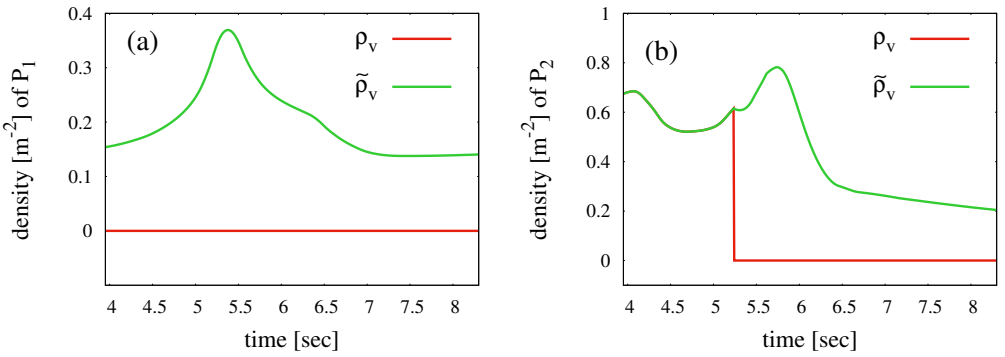

Figure 10: Time sequences of the density ρ_v (considering original Voronoi method) and $\tilde{\rho}_v$ (considering modified Voronoi cells clipped within the convex hull) for two typical pedestrians, (a) P_1 and (b) P_2 , denoted by the bigger black circle and triangle respectively in Figure 7.

It is worth mentioning here that density ρ_v, as defined by Equation (5), is apparently meaningless for agents on the edge of the groups, unless there are physical boundaries or at least imaginary boundary, such as the convex hull. The reason for this is quite obvious, which is that an infinitely large Voronoi cell of these agents would make the density value equal to zero, which however is not physical. So in the literature of pedestrian density estimation, whenever the Voronoi cell based method is employed, some bounding line has been used, even though arbitrary, to limit the infinitely large Voronoi cells near the boundary [52]. Otherwise, one is restricted to consider only the agents who are well within the bulk, i.e., whose Voronoi cells have no effect whether clipped or not.

From Figure 10(a) we can see that for pedestrian P_1 in Figure 7, the density ρ_v by original Voronoi method remains zero, which which does not account for the fact that P_1 is surrounded by pedestrians on one side. Whereas,

the density $\tilde{\rho}_v$ obtained by clipping the Voronoi cells by convex hull and including the angular sector corrections, produces a realistic estimate of density in the pedestrian's neighborhood.

On the other hand, for pedestrian P_2 in Figure 7 we get an interesting observation. The density estimate, as could be seen in Figure 10(b), remains the same for ρ_v and $\tilde{\rho}_v$ until about 5.25 sec. After this, ρ_v suddenly drops to zero, but $\tilde{\rho}_v$ continues to provide a realistic estimate of density. This can be understood from Figure 7. We see that for pedestrian P_2, the Voronoi cell remains well within the bulk at time 4.5 sec. As time progresses, this pedestrian moves upwards and remains located on the convex hull for the rest of the trial, naturally subtending an infinite Voronoi cell. It is only by clipping the cell by the convex hull and including the angular corrections that we obtain a physically possible density value. Hence the improvement in density estimation is brought about by $\tilde{\rho}_v$.

It is to be noted that the surface integral of Voronoi-based density field ρ_V (say, generically) gives the number of pedestrians. If we consider the surface $\mathcal{A}$ on which the integral is taken to be the union of Voronoi cells $\mathcal{C}$, i.e., $\mathcal{A} \equiv U\mathcal{C}$, then

$$\int^{\mathcal{A}} \rho_V d\mathbf{x} = \int^{U\mathcal{C}} \rho_V d\mathbf{x} = \sum_{\mathcal{C}} \frac{1}{A_{\mathcal{C}}} \times A_{\mathcal{C}} = N_{cells} = N_{peds}, \tag{8}$$

where $A_{\mathcal{C}}$ denotes the area of Voronoi cells. If a pedestrian is located on the convex hull, only part of their Voronoi cell is considered. This is a boundary effect, arising from the fact that we define density only within the group's interior, meaning pedestrians on the convex hull contribute only partially. If we were to extend the definition of density outside the convex hull, infinite cells would result in zero density, making the integral over an infinite cell undefined. Therefore, our method is primarily focused on measuring the density field within the group.

4. Conclusion and perspectives

In this paper we have presented a new computational algorithm based on Voronoi cells that makes it possible to estimate the density for individuals in the case of small groups moving without a spatial boundary. We begin by presenting an evaluation of the existing methods employed for density estimation in similar contexts, which highlights the limitations and drawbacks

of these approaches when calculating the density along the trajectory of a chosen pedestrian. The fact that these methods are parameter dependent makes them ill-defined for realistic, stable estimation of density in an individual's neighborhood. The density obtained using these methods contains systematic bias and fluctuations depending on the chosen parameter value. We then consider a Voronoi cell based method of density estimation [64] and propose a modification (Figure 6) for case of small pedestrian groups to obtain an unbiased, stable, parameter-independent estimate of the density. The resulting technique can be applied to small or large crowds, with or without physical boundaries.

In the literature on pedestrian density estimation, the XT method is often considered a rigorous method for constructing fundamental diagrams. However, calculating the pedestrian density using the XT method has several limitations. To begin with, an instantaneous measurement of density is not possible in the XT method. We see that the value of density at time t, actually depends not only on the current state of the system, but also on its state in the past and in the future. Specifically, the trajectory of the pedestrian under consideration, and those of its neighbors have to be taken into account within the time interval T, not just their positions at time t. This is a problem for highly non-stationary dynamics as in the crossing events considered here.

By contrast, in the Voronoi cell based density estimation, only the positions of pedestrians at time t are needed to calculate the instantaneous density of the neighborhood. The availability of data with longer trajectories is not essential for the Voronoi method to be useful.

Another drawback of the XT method for density estimation is its dependence on the parameters d_x and T. In our paper, we have demonstrated that density measurements using the XT method fluctuate significantly depending on the chosen parameters. There are no universally accepted values of d_x and T that should be used for density estimations. On the other hand, the advantages that we get by using Voronoi cell based density estimation is that it does not depend on the choice of parameter values, gives us a stable and realistic estimate of density in an individual's neighborhood, and has physical meaning for a wide variety of human crowd situations.

Our proposed method for estimation of pedestrian density could facilitate the construction of fundamental diagrams (FD) from the point of view of individual pedestrians along their trajectories. Thanks to our method, one is not restricted to considering the collective density of the whole group to

study the fundamental relation between density and velocity of the flow. This microscopic approach could potentially lead to the creation of more realistic models of crowd simulation, followed by more efficient methods of crowd management.

In our next endeavor we intend to study FDs for various conditions of the present data set. Several other methods can also allow to measure density along a trajectory, for example, using the harmonic sum of distances from a pedestrian to neighbors within the pedestrian's field of view [55], or considering the region where the convex hulls of the two crossing groups have an intersection, etc.

More generally, one has to keep in mind that at small scales a density cannot be defined in a strict way, as, for example, for a fluid. Indeed, a proper definition of density requires that there is a scale separation between, on the one hand, the individual scale and the dimension of the area in which density is computed by a proper averaging and, on the other hand, the scale on which density gradients occur or on which boundary effects become important. This is rarely the case for pedestrians and even less so for the small pedestrian groups that we consider here.

As explained in Section 1, while classical fundamental diagrams are plotted as a function of density, the notion of density could be enlarged in this context to an observable that would be relevant for the navigation of pedestrians. In this paper we focused on local density, however other definitions could be considered, closer to a perceived density, following [53]. Indeed, a pedestrian could experience the environment as empty even though there is one or more pedestrians present, simply due to having a large open space ahead. By contrast, an operator observing video footage might see that the room is not physically empty. This perspective is essential when analyzing density fluctuations over time, and can have significant implications for flow analysis and density measurements, particularly in the context of crowd dynamics. The perceived density certainly depends on neighboring pedestrians, but could depend more specifically on their relative positions (rear or front), on possible visual occlusions [74], on interpersonal distances [75], etc. We believe that more knowledge is needed about perceived density and how it affects pedestrian behavior, for example based on the visual field [76, 77].

One must thus keep in mind that the choice of the local density

plotted in the fundamental diagram is actually a hypothesis on the driving variable determining pedestrian dynamics. We shall explore various choices for this observable in our future research. For example, the free surface (or unoccupied area) could be a good candidate to replace density, by analogy with viscous fluids, for which free volume turned out to be more relevant than density for the dynamics.

One may also wonder, for pedestrians who are on the convex hull of a small group, how they react to the anisotropic density field around them. The Voronoi construction we detailed in this paper would give an appropriate tool to tackle this question. It would be especially interesting to couple it to the orientation of the pedestrians themselves.

Supplemental online material

S1 Video. Video of the modified Voronoi cells for all the pedestrians involved in the experimental trial of crossing flows shown in Figure 7, where we have shown snapshots of this video for 3 typical instances.

Funding

PM acknowledges financial support from Bretagne S.A.D., France and National Science Center (NCN), Poland through SONATA grant no. 2022/47/D/HS4/02576.

Disclosure Statement

The authors report that there are no competing interests to declare.

Data availability statement

The data set for crossing flows of pedestrians, which has been used in this research is available at `https://doi.org/10.5281/zenodo.5718430`. The computational method (in R) to use Voronoi cells with angular modifications to estimate individual densities in small pedestrian groups moving without physical boundaries is available at `https://doi.org/10.5281/zenodo.8138327`.

References

[1] T. D. Sweeny, S. Haroz, D. Whitney, Perceiving group behavior: sensitive ensemble coding mechanisms for biological motion of human crowds., Journal of Experimental Psychology: Human Perception and Performance 39 (2) (2013) 329.

[2] M. Haghani, M. Sarvi, Crowd behaviour and motion: Empirical methods, Transportation Research Part B: Methodological 107 (2018) 253–294.

[3] W. H. Warren, Collective motion in human crowds, Current directions in psychological science 27 (4) (2018) 232–240.

[4] C. Wang, S. Ni, W. Weng, Modeling human domino process based on interactions among individuals for understanding crowd disasters, Physica A: Statistical Mechanics and its Applications 531 (2019) 121781.

[5] M. Haghani, The knowledge domain of crowd dynamics: Anatomy of the field, pioneering studies, temporal trends, influential entities and outside-domain impact, Physica A: Statistical Mechanics and its Applications 580 (2021) 126145.

[6] A. Syed, S. P. Thampi, M. V. Panchagnula, Order-stampede transitions in human crowds: The role of individualistic and cooperative forces, Physica A: Statistical Mechanics and its Applications 598 (2022) 127349.

[7] G. Wang, T. Chen, H. Zheng, J. Wang, X. Hu, K. Deng, Z. Tao, N. Luo, Heterogeneous crowd dynamics considering the impact of personality traits under a fire emergency: A questionnaire & simulation-based approach, Physica A: Statistical Mechanics and its Applications 610 (2023) 128411.

[8] J. Chen, Q. Luo, Q. Wang, J. T. Lo, J. Ma, Experimental study on individual and crowd movement features around obstacles with different shape and size, Physica A: Statistical Mechanics and its Applications 645 (2024) 129797.

[9] D. C. Duives, W. Daamen, S. P. Hoogendoorn, State-of-the-art crowd motion simulation models, Transportation Research Part C: Emerging Technologies 37 (2013) 193–209.

[10] W. Van Toll, J. Pettré, Algorithms for microscopic crowd simulation: Advancements in the 2010s, in: Computer Graphics Forum, Vol. 40, Wiley Online Library, 2021, pp. 731–754.

[11] X. Zheng, T. Zhong, M. Liu, Modeling crowd evacuation of a building based on seven methodological approaches, Building and Environment 44 (3) (2009) 437–445.

[12] Y. Ma, R. K. K. Yuen, E. W. M. Lee, Effective leadership for crowd evacuation, Physica A: Statistical Mechanics and its Applications 450 (2016) 333–341.

[13] N. A. A. Bakar, M. A. Majid, K. A. Ismail, An overview of crowd evacuation simulation, Advanced Science Letters 23 (11) (2017) 11428–11431.

[14] Y. Li, M. Chen, Z. Dou, X. Zheng, Y. Cheng, A. Mebarki, A review of cellular automata models for crowd evacuation, Physica A: Statistical Mechanics and its Applications 526 (2019) 120752.

[15] C. Chen, T. Lu, W. Jiao, C. Shi, An extended model for crowd evacuation considering crowding and stampede effects under the internal crushing, Physica A: Statistical Mechanics and its Applications 625 (2023) 129002.

[16] J. R. Dyer, C. C. Ioannou, L. J. Morrell, D. P. Croft, I. D. Couzin, D. A. Waters, J. Krause, Consensus decision making in human crowds, Animal Behaviour 75 (2) (2008) 461–470.

[17] D. B. Saakian, The madness of crowds phenomenon in the collective decision-making by the cells, the cell's metacognition and cancer, Physica A: Statistical Mechanics and its Applications 492 (2018) 1408–1418.

[18] Y. Liu, Z. Mao, An experimental study on the critical state of herd behavior in decision-making of the crowd evacuation, Physica A: Statistical Mechanics and its Applications 595 (2022) 127087.

[19] J. Lorenz, H. Rauhut, F. Schweitzer, D. Helbing, How social influence can undermine the wisdom of crowd effect, Proceedings of the National Academy of Sciences 108 (22) (2011) 9020–9025.

[20] J. Becker, D. Brackbill, D. Centola, Network dynamics of social influence in the wisdom of crowds, Proceedings of the National Academy of Sciences 114 (26) (2017) E5070–E5076.

[21] V. Frey, A. Van de Rijt, Social influence undermines the wisdom of the crowd in sequential decision making, Management Science 67 (7) (2021) 4273–4286.

[22] P. Mavrodiev, F. Schweitzer, The ambigous role of social influence on the wisdom of crowds: An analytic approach, Physica A: Statistical Mechanics and its Applications 567 (2021) 125624.

[23] L. Pournajaf, L. Xiong, V. Sunderam, S. Goryczka, Spatial task assignment for crowd sensing with cloaked locations, in: 2014 IEEE 15th International Conference on Mobile Data Management, Vol. 1, IEEE, 2014, pp. 73–82.

[24] S. Abousamra, M. Hoai, D. Samaras, C. Chen, Localization in the crowd with topological constraints, in: Proceedings of the AAAI Conference on Artificial Intelligence, Vol. 35, 2021, pp. 872–881.

[25] V. Filingeri, K. Eason, P. Waterson, R. Haslam, Factors influencing experience in crowds–the participant perspective, Applied Ergonomics 59 (2017) 431–441.

[26] D. Helbing, L. Buzna, A. Johansson, T. Werner, Self-organized pedestrian crowd dynamics: Experiments, simulations, and design solutions, Transportation Science 39 (1) (2005) 1–24.

[27] D. King, S. Srikukenthiran, A. Shalaby, Using simulation to analyze crowd congestion and mitigation at canadian subway interchanges: case of bloor-yonge station, toronto, ontario, Transportation Research Record 2417 (1) (2014) 27–36.

[28] L. Huang, T. Chen, Y. Wang, H. Yuan, Congestion detection of pedestrians using the velocity entropy: A case study of love parade 2010 disaster, Physica A: Statistical Mechanics and its Applications 440 (2015) 200–209.

[29] C. Feliciani, K. Nishinari, Empirical analysis of the lane formation process in bidirectional pedestrian flow, Phys. Rev. E 94 (2016) 032304.

[30] C. Feliciani, K. Nishinari, Measurement of congestion and intrinsic risk in pedestrian crowds, Transportation Research Part C: Emerging Technologies 91 (2018) 124–155.

[31] F. Zanlungo, C. Feliciani, Z. Yücel, X. Jia, K. Nishinari, T. Kanda, A pure number to assess "congestion" in pedestrian crowds, Transportation Research Part C: Emerging Technologies 148 (2023) 104041.

[32] R. Kawaguchi, D. Yanagisawa, C. Feliciani, S. Nozaki, Y. Abe, M. Mita, K. Nishinari, Modeling and controlling congestion caused by a bottleneck in an overcrowded aquarium, Physica A: Statistical Mechanics and its Applications 615 (2023) 128547.

[33] W. Guo, X. Wang, X. Zheng, Lane formation in pedestrian counterflows driven by a potential field considering following and avoidance behaviours, Physica A: Statistical Mechanics and its Applications 432 (2015) 87–101.

[34] S. Cao, A. Seyfried, J. Zhang, S. Holl, W. Song, Fundamental diagrams for multidirectional pedestrian flows, Journal of Statistical Mechanics: Theory and Experiment 2017 (3) (2017) 033404.

[35] D. Zhang, H. Zhu, S. Hostikka, S. Qiu, Pedestrian dynamics in a heterogeneous bidirectional flow: Overtaking behaviour and lane formation, Physica A: Statistical Mechanics and its Applications 525 (2019) 72–84.

[36] A. S. Bodrova, F. A. Najim, N. Brilliantov, Lane formation in an active particle model with chirality for pedestrian traffic, Physica A: Statistical Mechanics and its Applications 643 (2024) 129796.

[37] S. Fang, C.-J. Jin, R. Jiang, D. Li, Simulating the bi-directional pedestrian flow under high densities by a floor field cellular automaton model, Physica A: Statistical Mechanics and its Applications 638 (2024) 129626.

[38] M. Muramatsu, T. Nagatani, Jamming transition in two-dimensional pedestrian traffic, Physica A: Statistical Mechanics and its Applications 275 (1-2) (2000) 281–291.

[39] T. Nagatani, Dynamical transition in merging pedestrian flow without bottleneck, Physica A: Statistical Mechanics and its Applications 307 (3-4) (2002) 505–515.

[40] Y. Tajima, T. Nagatani, Clogging transition of pedestrian flow in t-shaped channel, Physica A: Statistical Mechanics and its Applications 303 (1-2) (2002) 239–250.

[41] T. Nagatani, Freezing transition in bi-directional ca model for facing pedestrian traffic, Physics Letters A 373 (33) (2009) 2917–2921.

[42] Y. Liu, X. Ma, Y. Tao, L. Dong, X. Ding, X. Qiu, Numerical investigation on the impact of obstacles on phase transition in pedestrian counter-flow, Physica A: Statistical Mechanics and its Applications 635 (2024) 129499.

[43] L. Wang, S. Shen, A decay model for the fundamental diagram of pedestrian movement, Physica A: Statistical Mechanics and its Applications 531 (2019) 121739.

[44] L. Lian, R. Ye, L. Xia, W. Song, J. Zhang, X. Li, Pedestrian dynamics in single-file merging flows, Physica A: Statistical Mechanics and its Applications 600 (2022) 127549.

[45] S. Paetzke, M. Boltes, A. Seyfried, Influence of individual factors on fundamental diagrams of pedestrians, Physica A: Statistical Mechanics and its Applications 595 (2022) 127077.

[46] E. Cristiani, M. Menci, A. Malagnino, G. Amaro, An all-densities pedestrian simulator based on a dynamic evaluation of the interpersonal distances, Physica A: Statistical Mechanics and its Applications 616 (2023) 128625.

[47] T. Zeng, Y. Wei, Z. Hu, Y. Ma, Comparison study in single-file pedestrian flow dynamics: Foot motion perspective versus head motion perspective, Physica A: Statistical Mechanics and its Applications 629 (2023) 129177.

[48] M. Rangel-Galván, A. L. Ballinas-Hernández, V. Rangel-Galván, Thermo-inspired model of self-propelled hard disk agents for heterogeneous bidirectional pedestrian flow, Physica A: Statistical Mechanics and its Applications 635 (2024) 129500.

[49] N. Geroliminis, C. F. Daganzo, Existence of urban-scale macroscopic fundamental diagrams: Some experimental findings, Transportation Research Part B: Methodological 42 (9) (2008) 759–770.

[50] M. Keyvan-Ekbatani, A. Kouvelas, I. Papamichail, M. Papageorgiou, Exploiting the fundamental diagram of urban networks for feedback-based gating, Transportation Research Part B: Methodological 46 (10) (2012) 1393–1403.

[51] A. Seyfried, B. Steffen, W. Klingsch, M. Boltes, The fundamental diagram of pedestrian movement revisited, Journal of Statistical Mechanics: Theory and Experiment (2005) P10002.

[52] D. Helbing, A. Johansson, H. Z. Al-Abideen, Dynamics of crowd disasters: An empirical study, Phys. Rev. E 75 (2007) 046109.

[53] B. Steffen, A. Seyfried, Methods for measuring pedestrian density, flow, speed and direction with minimal scatter, Physica A: Statistical Mechanics and its Applications 389 (9) (2010) 1902–1910.

[54] L. Schauer, M. Werner, P. Marcus, Estimating crowd densities and pedestrian flows using wi-fi and bluetooth, in: Proceedings of the 11th International Conference on Mobile and Ubiquitous Systems: Computing, Networking and Services, 2014, pp. 171–177.

[55] D. C. Duives, W. Daamen, S. P. Hoogendoorn, Quantification of the level of crowdedness for pedestrian movements, Physica A: Statistical Mechanics and its Applications 427 (2015) 162–180.

[56] A. S. Rao, J. Gubbi, S. Marusic, M. Palaniswami, Estimation of crowd density by clustering motion cues, The Visual Computer 31 (11) (2015) 1533–1552.

[57] S. A. M. Saleh, S. A. Suandi, H. Ibrahim, Recent survey on crowd density estimation and counting for visual surveillance, Engineering Applications of Artificial Intelligence 41 (2015) 103–114.

[58] A. Tordeux, J. Zhang, B. Steffen, A. Seyfried, Quantitative comparison of estimations for the density within pedestrian streams, Journal of Statistical Mechanics: Theory and Experiment (2015) P06030.

[59] K. Nagao, D. Yanagisawa, K. Nishinari, Estimation of crowd density applying wavelet transform and machine learning, Physica A: Statistical Mechanics and its Applications 510 (2018) 145–163.

[60] X. Ding, F. He, Z. Lin, Y. Wang, H. Guo, Y. Huang, Crowd density estimation using fusion of multi-layer features, IEEE Transactions on Intelligent Transportation Systems 22 (8) (2020) 4776–4787.

[61] S. Marisamynathan, S. Lakshmi, Method to determine pedestrian level of service for sidewalks in indian context, Transportation Letters 10 (5) (2018) 294–301. doi:10.1080/19427867.2016.1264668.

[62] D. Wei, W. Kumfer, D. Wu, H. Liu, Traffic queuing at unsignalized crosswalks with probabilistic priority, Transportation Letters 10 (3) (2018) 129–143. doi:10.1080/19427867.2016.1236069.

[63] J. Zhang, W. Klingsch, T. Rupprecht, A. Schadschneider, A. Seyfried, Empirical study of turning and merging of pedestrian streams in t-junction (2011). doi:10.48550/ARXIV.1112.5299.

[64] A. Nicolas, M. Kuperman, S. Ibañez, S. Bouzat, C. Appert-Rolland, Mechanical response of dense pedestrian crowds to the crossing of intruders, Scientific Reports 9 (2019) 105.

[65] L. C. Edie, Discussion of traffic stream measurements and definitions., Proceedings of the Second International Symposium on the Theory of Traffic Flow, London (1963) 139–154.

[66] N. W. F. Bode, M. Chraibi, S. Holl, The emergence of macroscopic interactions between intersecting pedestrian streams, Transportation Research Part B: Methodological 119 (2019) 197–210.

[67] M. Saberi, H. S. Mahmassani, Exploring areawide dynamics of pedestrian crowds: Three-dimensional approach, Transportation Research Record 2421 (1) (2014) 31–40.

[68] A. Jelić, C. Appert-Rolland, S. Lemercier, J. Pettré, Properties of pedestrians walking in line – fundamental diagrams, Physical Review E 85 (2012) 036111.

[69] C. Appert-Rolland, J. Pettré, A.-H. Olivier, W. Warren, A. Duigo-Majumdar, E. Pinsard, A. Nicolas, Experimental study of collective pedestrian dynamics, Collective Dynamics 5 (2020) 1–8.

[70] P. Mullick, S. Fontaine, C. Appert-Rolland, A.-H. Olivier, W. H. Warren, J. Pettré, Analysis of emergent patterns in crossing flows of pedestrians reveals an invariant of 'stripe' formation in human data, PLoS Computational Biology 18(6) (2022) e1010210.

[71] R.-Y. Guo, S. C. Wong, H.-J. Huang, P. Zhang, W. H. K. Lam, A microscopic pedestrian-simulation model and its application to intersecting flows, Physica A: Statistical Mechanics and its Applications 389 (2010) 515–526.

[72] F. Zanlungo, C. Feliciani, Z. Yücel, K. Nishinari, T. Kanda, Macroscopic and microscopic dynamics of a pedestrian cross-flow: Part I, experimental analysis, Safety Science 158 (2023) 105953.

[73] F. Zanlungo, C. Feliciani, Z. Yücel, K. Nishinari, T. Kanda, Macroscopic and microscopic dynamics of a pedestrian cross-flow: Part II, modelling, Safety Science 158 (2023) 105969.

[74] G. C. Dachner, T. D. Wirth, E. Richmond, W. H. Warren, The visual coupling between neighbours explains local interactions underlying human 'flocking', Proceedings of the Royal Society B 289 (2022) 20212089.

[75] P. Geoerg, J. Schumann, M. Boltes, M. Kinateder, How people with disabilities influence crowd dynamics of pedestrian movement through bottlenecks, Scientific Reports 12 (2022) 14273.

[76] W. Poel, C. Winklmayr, P. Romanczuk, Spatial structure and information transfer in visual networks, Frontiers in Physics 9 (2021) 716576.

[77] T. D. Wirth, G. C. Dachner, K. W. Rio, W. H. Warren, Is the neighborhood of interaction in human crowds metric, topological, or visual?, PNAS nexus 2 (5) (2023) pgad118.